Grid-Based Quaternion Filter for SO(3) Estimation

Kailai Li, Florian Pfaff, and Uwe D. Hanebeck

***Abstract*— A novel discrete Bayesian filtering scheme is proposed on the manifold of unit quaternions for rotation estimation. Existing quaternion filters rely on specific distributions (typically the Bingham distribution) to model the uncertainty in a parametric form. The scheme proposed in this paper allows non-parametric modeling of the underlying uncertainty using Dirac mixtures located on a hyperspherical grid. The grid is generated by first discretizing the tangent space layer-wise w.r.t. spherical coordinates. Then, the on-tangent-space grid is mapped back to the manifold via the exponential map. The on-manifold grid of quaternions is deployed in a discrete Bayesian filtering scheme. We evaluate the proposed grid-based quaternion filter for recursive rotation estimation with simulations. Results show that the tracking performance of the proposed approach is superior to Bingham-based quaternion filters.**

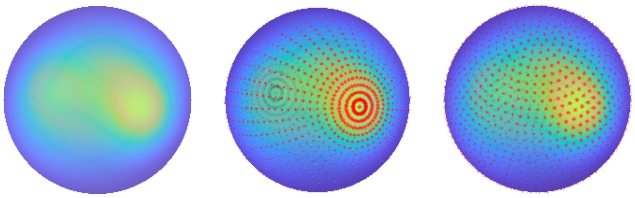

(a) density (b) MCG (c) SEP

Fig. 1: Example of grid-based modeling for uncertain states on (hyper-)spheres as introduced in Sec. III. The antipodally symmetric density on $\mathbb{S}^2$ shown in (a) is represented by Dirac mixture on a MCG in (b) and a grid given by the SEP in (c). Grid points (red) are depicted with sizes proportional to their weights.

I. Introduction

Estimation of rigid body rotation is ubiquitous and plays a crucial role in many control-related estimation tasks [1]–[4]. Due to the inherent nonlinearity of the underlying group structure, namely the special orthogonal group SO(3) , deriving robust and accurate recursive rotation estimators is non-trivial. Also, spatial rotations can be parameterized in various ways. Euler angles, for instance, provide a minimal representation and are among the most popular ones. However, they suffer from the issue of 'gimbal lock' [5]. This ambiguity can be overcome via overparameterization with the well-known 3×3 rotation matrices. However, they introduce a large degree of redundancy (nine elements are used to represent three DoF), leading to higher memory consumption and potential numerical instability. As a reparameterization of the axis-angle representation, unit quaternions can be formulated as four-dimensional vectors, resulting in only one degree of redundancy and no ambiguity. In this paper, we employ unit quaternions to represent spatial rotations and propose a recursive Bayesian filter based thereon. Recursive filtering on unit quaternions requires handling the nonlinear manifold structure, i.e., the three-dimensional unit hypersphere $\mathbb{S}^3 \subset \mathbb{R}^4$. Existing approaches usually employ nonlinear filtering techniques, e.g., the extended Kalman filter (EKF) [6] or unscented Kalman filter (UKF) [7], in a locally linearized space [8]–[10]. Such adaptations to the manifold structure can often bring additional numerical issues. Further, the adapted approaches still suffer from existing problems of the original filters, such as divergence due to poor initial estimates and tedious parameter tuning [11], [12]. Also, the linearization itself relies on the assumption of local perturbation, which can be violated under large initial uncertainty and fast rotation. Direct on-manifold modeling of uncertain rotations is enabled by employing distributions from directional statistics [13], [14]. More specifically, the antipode of a unit quaternion represents the same rotation, thus should be endowed with the same density. The Bingham distribution on $\mathbb{S}^3$ has therefore become a popular tool for modeling uncertain quaternions, as its probability density function (PDF) $f_{\mathcal{B}} = 1/N_c \cdot \exp\left(\mathbf{x}^\top \mathbf{C}\, \mathbf{x}\right)$ inherently guarantees the antipodal symmetry. Based on this distribution, corresponding recursive quaternion estimators were proposed.

Existing Bingham-based quaternion filtering methods usually follow the sampling-approximation scheme. Samples are propagated through system dynamics or updated via the likelihood function. Afterward, the prior or posterior Bingham density can be approximated from the samples by means of moment-matching (second order). Random sampling schemes for the Bingham distribution have been proposed [15] and deployed in orientation as well as pose estimation [16]–[19]. However, they cannot guarantee repeatable results and are computationally inefficient. In [20], a deterministic sampling approach was proposed following the idea of the unscented transform, which approximates the underlying Bingham density up to the second order for moment matching. The deterministic sampling scheme guarantees repeatable results and has shown improved tracking accuracy as well as computational efficiency compared with its random counterpart. One drawback of this deterministic sampling method is the limited performance for nonlinear rotation estimation, as samples of fixed and limited quantity (seven sigma points of unit quaternions) can easily degenerate when updated with a peaky likelihood function.

This work is supported by the German Research Foundation (DFG) under grant HA 3789/16-1. The authors are with the Intelligent Sensor-Actuator-Systems Laboratory (ISAS), Institute for Anthropomatics and Robotics, Karlsruhe Institute of Technology (KIT), Germany. E-Mails:{kailai.li, florian.pfaff, uwe.hanebeck}@kit.edu

Therefore, flexible deterministic sampling schemes were proposed in [21], [22], which approximate higher-order shape information of the Bingham distribution with a freely given sample size. Here, uniformly weighted samples are drawn by minimizing certain distance metrics between the Dirac mixture given by the samples and the underlying Bingham density under the constraint of the unscented transform (for moment matching of second order). With an adequate sample size, better tracking accuracy and robustness were shown for nonlinear rotation estimation. Generating large numbers of samples, however, inevitably involves high-dimensional optimizations, bringing issues regarding computational cost and sampling stability.

The aforementioned filtering techniques, regardless of whether they were proposed in on-manifold fashions or not, all rely on parametric modeling of uncertain quaternions. However, this assumption is usually violated for complex and nonlinear systems. Another downside to employing the Bingham distribution lies in the computation of the normalization constant N_c as no analytic solution exists. To avoid computationally expensive numerical integration, precomputed and memory-intensive lookup tables [15], [23] were used. Further, an acceleration thereof based on saddle point approximation or the Gauss-Newton approach [24] was proposed. However, the extra computational expense cannot be ignored since the distribution has to be approximated whenever an estimate is desired (e.g., in every prediction and update step). Also, the optimization-based approach is sometimes numerically unstable [25].

Considering that the hypersphere is compact and bounded, a grid can be deployed to discretize the manifold of unit quaternions and model the underlying uncertainty in a non-parametric form. The concept of a grid-based filter was presented first in the Wonham filter [26]. A similar modeling approach and discrete Bayesian filtering scheme on periodic and bounded domains were proposed in [27], [28]. By discretizing the circular state space with a grid, the uncertainty of angular variables can be interpreted by either piece-wise constant densities or the Dirac mixtures. Though promising results were shown for planar rotation and rigid body motion estimation, there exists no work for discrete quaternion filtering on the hypersphere $\mathbb{S}^3$. In fact, grid generation on $\mathbb{S}^3$ in the context of quaternion filtering is non-trivial. Naïvely discretizing high-dimensional spaces (e.g., equidistant grids) usually requires a high resolution to reach the desired tracking accuracy and robustness. Also, the antipodal symmetry of quaternion states should be considered for grid generation and the design of the filtering scheme. Furthermore, the propagated Dirac mixture needs to be fused into the grid with consideration of the manifold structure.

In this work, we propose a novel grid-based Bayesian filtering scheme on unit quaternion for nonlinear rotation estimation. The grid is generated via on-tangent-space discretization w.r.t. spherical coordinates followed by the exponential map. The on-manifold uncertainty is then directly modeled by a Dirac mixture at the grid points. Based on the generated grid, a corresponding quaternion filter is proposed and evaluated for SO(3) estimation. More specifically, we highlight the following contributions.

- A mode-centric grid generation scheme is proposed for discretization of the unit quaternion manifold with consideration of the underlying distribution.
- On-manifold uncertainty of unit quaternions is modeled in a non-parametric way based on the Dirac mixture at hyperspherical grid points.
- A novel grid-based quaternion filter, which shows improved robustness and accuracy for nonlinear rotation estimation, is proposed.

The remainder of the paper is structured as follows. In Sec. II, preliminaries about the quaternion representation of spatial rotations and the corresponding manifold geometry are introduced. The novel grid generation and manipulation approaches are given in Sec. III, after which the discrete quaternion filter is proposed in Sec. IV. The evaluation is performed in Sec. V for nonlinear rotation estimation. Finally, the work is concluded in Sec. VI.

II. Preliminaries

A. Quaternion Arithmetics and Rotation Parameterization

By definition, quaternions parameterize spatial rotations in the form

$$\mathbf{x} = [\,\cos(\theta/2)\,,\, \mathbf{n}^\top \sin(\theta/2)\,]^\top := [\,x_0, x_1, x_2, x_3\,]^\top\,, \quad (1)$$

with the unit vector $\mathbf{n}$ being the rotation axis around which a rotation of angle θ is performed. Aggregation of two quaternions is done via the Hamilton product. It can also be written as ordinary matrix-vector multiplications according to $\mathbf{x} \otimes \mathbf{y} = \mathcal{Q}^{\llcorner}_{\mathbf{x}}\, \mathbf{y} = \mathcal{Q}^{\lrcorner}_{\mathbf{y}}\, \mathbf{x}$, with

$$\mathcal{Q}^{\llcorner}_{\mathbf{x}} = \begin{bmatrix} x_0 & -x_1 & -x_2 & -x_3 \\ x_1 & x_0 & -x_3 & x_2 \\ x_2 & x_3 & x_0 & -x_1 \\ x_3 & -x_2 & x_1 & x_0 \end{bmatrix},\ \mathcal{Q}^{\lrcorner}_{\mathbf{y}} = \begin{bmatrix} y_0 & -y_1 & -y_2 & -y_3 \\ y_1 & y_0 & y_3 & -y_2 \\ y_2 & -y_3 & y_0 & y_1 \\ y_3 & y_2 & -y_1 & y_0 \end{bmatrix} \quad (2)$$

denoting the matrix form of quaternions when being multiplied from left and right side, respectively. The norm of a quaternion is then defined as $\sqrt{\mathbf{x} \otimes \mathbf{x}^*}$ with $\mathbf{x}^* = \operatorname{diag}(1, -1, -1, -1)\, \mathbf{x}$ being the conjugate of $\mathbf{x}$. Therefore, quaternions in (1) representing spatial rotations are of unit norm, and are thus called unit quaternions. Also, they are of unit length in the Euclidean space $\mathbb{R}^4$, i.e., $\|\mathbf{x}\| = 1$.

The manifold $\mathbb{S}^3$ comprises all vectors in $\mathbb{R}^4$ of unit length. Note the matrix form of unit quaternions as shown in (2) thus belongs to the four-dimensional rotation group, i.e., $\mathcal{Q}^{\llcorner}_{\mathbf{x}}, \mathcal{Q}^{\lrcorner}_{\mathbf{x}} \in \mathrm{SO}(4), \forall\, \mathbf{x} \in \mathbb{S}^3$. Also, it can be easily derived that inverting a unit quaternion corresponds to transposing its matrix form, e.g., $\mathcal{Q}^{\llcorner}_{\mathbf{x}^{-1}} = \mathcal{Q}^{\llcorner\top}_{\mathbf{x}}$. Given the definition in (1), any point $\mathbf{s} \in \mathbb{R}^3$ can be rotated according to

$$\mathbf{s}' = \left(\mathbf{x} \otimes [\,0, \mathbf{s}^\top]^\top \otimes \mathbf{x}^*\right)_{2:4}\,. \quad (3)$$

Here, we add 0 before $\mathbf{s}$ for adaptation to quaternion arithmetics and take out the last three elements $(\cdot)_{2:4}$ from the products to obtain the rotated vector $\mathbf{s}'$. The hypersphere $\mathbb{S}^3$ is therefore a double covering of the SO(3) group. As mentioned in Sec. I, the Bingham distribution can be employed for parametric stochastic modeling of uncertain

unit quaternions as its density is antipodally symmetric by definition. The symmetry should also be considered for non-parametric modeling schemes with hyperspherical grids.

B. Geometric Structure of Unit Quaternion Manifold

The unit quaternion manifold is a compact Riemannian manifold with constant curvature and its structure can be investigated based on the hyperspherical geometry [21], [22]. Given a unit quaternion $\boldsymbol{\nu} \in \mathbb{S}^3$, a tangent plane $\mathcal{T}_{\boldsymbol{\nu}}\mathbb{S}^3$ can be located at this point such that all on-tangent-plane elements are orthogonal to $\boldsymbol{\nu}$. Any on-manifold $\mathbf{x} \in \mathbb{S}^3$ can be mapped to $\mathcal{T}_{\boldsymbol{\nu}}\mathbb{S}^3$ via the logarithm map defined as follows

$$\tilde{\mathbf{x}} = \mathrm{Log}_{\boldsymbol{\nu}}(\mathbf{x}) = (\mathbf{x} - \cos(\alpha)\,\boldsymbol{\nu})\,\alpha/\sin(\alpha) \in \mathcal{T}_{\boldsymbol{\nu}}\mathbb{S}^3\,. \quad (4)$$

The formula $\alpha = \mathrm{acos}(\boldsymbol{\nu}^\top \mathbf{x})$ can be used to calculate the arc length α between $\boldsymbol{\nu}$ and $\mathbf{x}$. As the inverse operation, any on-tangent-plane point $\tilde{\mathbf{x}} \in \mathcal{T}_{\boldsymbol{\nu}}\mathbb{S}^3$ can be mapped back to the manifold via

$$\mathbf{x} = \mathrm{Exp}_{\boldsymbol{\nu}}(\tilde{\mathbf{x}}) = \cos(\|\tilde{\mathbf{x}}\|)\,\boldsymbol{\nu} + \tilde{\mathbf{x}}\sin(\|\tilde{\mathbf{x}}\|)/\|\tilde{\mathbf{x}}\| \in \mathbb{S}^3\,. \quad (5)$$

Note that both operations are geodesic-preserving. For instance, the arc length (geodesic on spheres) between $\boldsymbol{\nu}$ and $\mathbf{x}$ equals their on-tangent-plane distance after logarithm map, i.e., $\mathrm{acos}(\boldsymbol{\nu}^\top \mathbf{x}) = \|\mathrm{Log}_{\boldsymbol{\nu}}(\mathbf{x})\|$. When considering the tangent plane at the identity unit quaternion $\mathbb{1} = [\,1, 0, 0, 0\,]^\top$, the corresponding logarithm map is derived as

$$\tilde{\mathbf{x}} = \mathrm{Log}_{\mathbb{1}}(\mathbf{x}) = [\,0,\, \tfrac{\theta}{2}\,\mathbf{n}^\top\,]^\top \in \mathcal{T}_{\mathbb{1}}\mathbb{S}^3\,,$$

with $\mathbf{x} = [\,\cos(\theta/2),\, \mathbf{n}^\top \sin(\theta/2)\,]^\top \in \mathbb{S}^3$. Furthermore, any logarithm and exponential map can also be performed at the identity unit quaternion according to the following rule

$$\begin{aligned}\tilde{\mathbf{x}} &= \mathrm{Log}_{\boldsymbol{\nu}}(\mathbf{x}) = \boldsymbol{\nu} \otimes \mathrm{Log}_{\mathbb{1}}(\boldsymbol{\nu}^{-1} \otimes \mathbf{x}) \in \mathcal{T}_{\boldsymbol{\nu}}\mathbb{S}^3\,,\\ \mathbf{x} &= \mathrm{Exp}_{\boldsymbol{\nu}}(\tilde{\mathbf{x}}) = \boldsymbol{\nu} \otimes \mathrm{Exp}_{\mathbb{1}}(\boldsymbol{\nu}^{-1} \otimes \tilde{\mathbf{x}}) \in \mathbb{S}^3\,.\end{aligned}$$

The equations above essentially denote an inverse rotation of $\mathcal{Q}_{\boldsymbol{\nu}}^{\mathrm{L}}$ followed by the desired operation on $\mathcal{T}_{\mathbb{1}}\mathbb{S}^3$, after which a rotation back to $\boldsymbol{\nu}$ is performed. Moreover, as the vector $\mathbf{n}$ is of unit length and $\theta \in [\,0, \pi\,]$ (consider antipodal symmetry), the tangent space at a unit quaternion is essentially a ball of radius $\pi/2$.

III. Grid-based Stochastic Modeling of Uncertain Unit Quaternions

In this section, we propose to stochastically model the uncertainty of unit quaternions with grid-based Dirac mixtures.

A. Mode-Centric Grid (MCG)-Based Stochastic Modeling

Approaches based on different principles have been proposed for generating grids on hyperspheres. One popular solution given in [29] generates a hyperspherical grid by partitioning the hypersphere into equal-area patches, resulting in quasi-equidistant grid points. This spherical equal partitioning (SEP) approach has been employed as the deterministic sampling scheme for a linear regression Kalman filter in [30]. Though the generated grid points evenly cover the hypersphere, the antipodal symmetry of unit quaternions is not taken into consideration. More importantly, naïvely employing this approach to discretize the unit quaternion manifold usually requires a high grid resolution for an effective modeling of hyperspherical uncertainty, leading to unsatisfactory memory as well as computational efficiencies. In fact, the underlying density for quaternions on $\mathbb{S}^3$ cannot be uniform in reality. Considering the information geometry of the underlying uncertainty, a mode-centric grid (MCG), which has a higher resolution in the vicinity of the mode, is therefore proposed.

Algorithm 1: Mode-Centric Grid (MCG) Generation

Input: layer L, per-layer resolution M, mode $\boldsymbol{\nu}$
Output: hyperspherical grid set $\mathbb{B}$

1 $\mathbb{B} \leftarrow \emptyset$;
2 $\{\tilde{\boldsymbol{\beta}}_m\}_{m=1}^{M} \leftarrow \mathtt{SEP}\left(\mathbb{S}^2, M\right)$;
3 **for** $l \leftarrow 1$ ***to*** L **do**
4 **for** $m \leftarrow 1$ **to** M **do**
5 $\boldsymbol{\beta} \leftarrow \boldsymbol{\nu} \otimes \mathrm{Exp}_{\mathbb{1}}\left(\frac{\pi l}{2L}[\,0, \tilde{\boldsymbol{\beta}}_m^\top\,]^\top\right)$;
6 $\mathbb{B} \leftarrow \mathbb{B} \cup \boldsymbol{\beta}$;
7 **end**
8 **end**
9 $\mathbb{B} \leftarrow \mathbb{B} \cup \boldsymbol{\nu}$;
10 **return** $\mathbb{B}$;

When observed w.r.t. spherical coordinates, the ball-shaped tangent plane can be discretized layer-wise by a range of radii according to a certain resolution L. As shown in Alg. 1, the SEP algorithm [29] is hereby applied, generating M grid points at each layer (Alg. 1, line 2). Afterward, on-tangent-plane grid points are mapped to the hypersphere via the exponential map at the given mode $\boldsymbol{\nu}$ (Alg. 1, line 5) such that the set of on-manifold grid points $\mathbb{B} \subset \mathbb{S}^3$ can be obtained. In the end, the mode is also incorporated (Alg. 1, line 9) and the grid size (cardinality $|\mathbb{B}|$) equals $M \times L + 1$.

As each spherical layer of different area is discretized with the same resolution on the tangent plane, the grid after the exponential map is mode-concentrating. One may argue that the state space, namely the hypersphere, is not evenly covered by the grid set and the mode-centric grid shape has an implicit assumption of unimodality for the underlying PDF. However, such a design does allow for representing multimodal uncertainties of unit quaternions since the grid covers the entire state space. Furthermore, there are usually large gradients of the underlying density around the mode. Thus, its vicinity needs to be covered by more grid points. A mode-centric grid shape can alleviate grid degeneration issues for strong nonlinearities. In many applications, a single state estimate is preferable for instant decision making (e.g., a robot needs a certain estimate of its current orientation for path planing). The proposed mode-centric grid (MCG) can hereby provide a good trade-off between tracking accuracy and computational cost.

Given the discretized state space, the Dirac delta function can be placed at each grid point such that an underlying density can be represented by the Dirac mixture $\sum_i \omega_i\,\delta(\mathbf{x} - \boldsymbol{\beta}_i)$. Here, the weights w_i represent the density

at each grid point $\boldsymbol{\beta}_i$ and $\sum_i \omega_i = 1$ holds. Fig. 1 further illustrates the grid-based representation of a synthesized spherical density that is antipodally symmetric. With a grid resolution of $L \times M + 1 = 20 \times 40 + 1 = 801$ points on the hemisphere, the proposed MCG gives a more efficient discrete modeling of the underlying density than the SEP-based approach using the same resolution. Also, the SEP was not proposed for representing antipodally symmetric density and has to be applied for the whole spherical domain, resulting in double memory expense (with $801 \times 2 = 1602$ grid points). Fig. 2 further demonstrates the MCG-based modeling approach using different grid resolutions. With a higher resolution, the grid-based representation tends to retain more details of the underlying density.

B. Grid Transport

When performing recursive estimation on unit quaternion states, the mode of the estimated density is constantly changing. The grid should then be transported and centralized around the updated mode without distorting the grid shape. For that, we deploy the hyperspherical geometry introduced in II-A. When the mode is updated from $\boldsymbol{\nu}_1$ to $\boldsymbol{\nu}_2$, the grid is transported accordingly as

$$\boldsymbol{\beta}' = \boldsymbol{\beta} \otimes \boldsymbol{\nu}_1^{-1} \otimes \boldsymbol{\nu}_2 = \mathcal{Q}_{\boldsymbol{\nu}_2}^{\lrcorner} \, \mathcal{Q}_{\boldsymbol{\nu}_1}^{\lrcorner\top} \boldsymbol{\beta} := \mathcal{R}_{\boldsymbol{\nu}_1}^{\boldsymbol{\nu}_2} \, \boldsymbol{\beta} \tag{6}$$

with $\mathcal{R}_{\boldsymbol{\nu}_1}^{\boldsymbol{\nu}_2}$ belonging to the SO(4) rotation group. As the transportation is essentially a rigid body rotation in $\mathbb{R}^4$, the grid shape is preserved. Moreover, the transporting is derived from the Hamilton product, under which the manifold $\mathbb{S}^3$ is closed. Therefore, the grid points are confined to the hypersphere after transportation.

IV. Grid-based Quaternion Filtering Framework

Using the proposed MCG-based Dirac mixture, a Bayesian filtering scheme for quaternion-based orientation estimation can be established. Unlike existing quaternion filters, in which noise distributions are required in parametric forms, more flexible problem set-ups are hereby allowed. For instance, the system dynamics can be formulated as $\mathbf{x}_{k+1} = a\left(\mathbf{x}_k, \mathbf{w}_k\right)$ with unit quaternions $\mathbf{x}_{k+1}, \mathbf{x}_k \in \mathbb{S}^3$ being orientation states and $\mathbf{w}_k \in \mathbb{W}$ the system noise[1]. Note that no assumption of density in parametric form is required for the noise term and the transition function $a : \mathbb{S}^3 \times \mathbb{W} \mapsto \mathbb{S}^3$ can be formulated in a more intuitive way (e.g., directly from kinematics of actuators). Similarly, the measurement model $\mathbf{z}_k = h\left(\mathbf{x}_k, \mathbf{v}_k\right)$ is given in a generic form with $\mathbf{z}_k \in \mathbb{Z}$ denoting the measurement and $\mathbf{v}_k \in \mathbb{V}$ the measurement noise. The observation function $h : \mathbb{S}^3 \times \mathbb{V} \mapsto \mathbb{Z}$ can be directly modeled according to the sensory modality without density assumptions or adaptations to specific filters.

Throughout the filtering scheme, the estimate of the quaternion state is represented by the weighted grid points. The full MCG-based quaternion filtering approach is given in Alg. 2. For the prediction step, the prior can be derived as

$$f_{\mathrm{p}}(\mathbf{x}_{k+1}) \approx \sum_{i=1}^{n} \sum_{r=1}^{n_{\mathrm{w}}} \omega_i^k \, \omega_r^{\mathrm{w}} \, \delta\left(\mathbf{x}_{k+1} - a\left(\boldsymbol{\beta}_i^k, \boldsymbol{\sigma}_r\right)\right) ,$$

[1]Without loss of generality, we ignore system inputs for better readability.

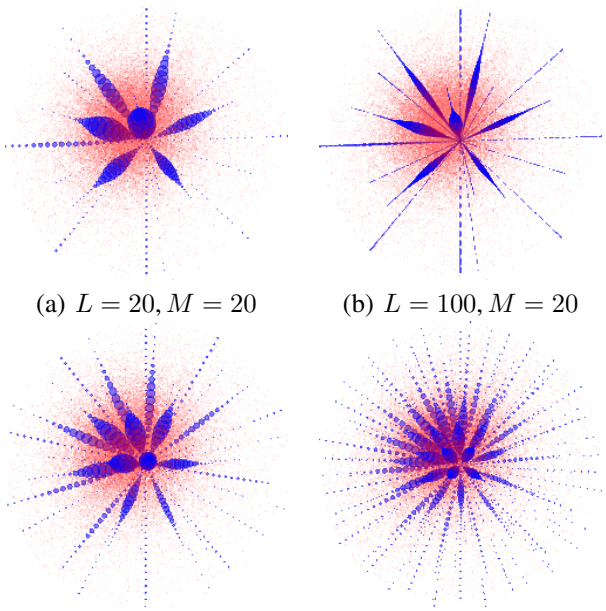

(a) $L = 20, M = 20$ (b) $L = 100, M = 20$

(c) $L = 20, M = 40$ (d) $L = 20, M = 100$

Fig. 2: Grid-based modeling of hyperspherical uncertainty using different grid resolutions. Uncertain unit quaternions (red dots) are randomly drawn from a Bingham distribution with mode $\boldsymbol{\nu}$ and plotted on the $\mathcal{T}_{\boldsymbol{\nu}}\mathbb{S}^3$ via logarithm map. The underlying uncertainty is represented by weighted MCG points (blue dots).

i.e., grid points of $\mathbb{B}_k = \{\boldsymbol{\beta}_i^k\}_{i=1}^n$ are propagated by noise particles $\{\boldsymbol{\sigma}_r\}_{r=1}^{n_{\mathrm{w}}}$ through the transition function (Alg. 2 line 1). A detailed derivation is provided in Appendix A.

Two side effects occur when propagating the grid points. First, the hyperspherical grid is no longer centralized at the mode. This can be fixed by transporting the grid from the old mode to the current one as shown in (6). The mode-centric grid can thus be updated without shape distortion (shown in Alg. 2, lines 2–4). Second, the propagated points almost surely do not land on the grid again, i.e., $a\left(\boldsymbol{\beta}_i^k, \boldsymbol{\sigma}_r\right) \notin \mathbb{B}_{k+1}$. Therefore, the propagated grid points need to be approximated by the updated grid. For that, we reset the weights of the prior grid and reallocate the propagated weight $\omega_i^k \omega_r^{\mathrm{w}}$ to neighboring grid points $\{\boldsymbol{\beta}_{\lambda_s}^{k+1}\}_{s=1}^{\Lambda}$ according to a metric $\mathcal{D}$ in relation to the distance between them (shown in Alg. 2, lines 5–11). The weight added to the neighboring points is thus

$$\frac{\mathcal{D}\left(\boldsymbol{\beta}_{\lambda_s}^{k+1}, \, a\left(\boldsymbol{\beta}_i^k, \boldsymbol{\sigma}_r\right)\right)}{\sum_{s=1}^{\Lambda} \mathcal{D}\left(\boldsymbol{\beta}_{\lambda_s}^{k+1}, \, a\left(\boldsymbol{\beta}_i^k, \boldsymbol{\sigma}_r\right)\right)} \omega_i^k \, \omega_r^{\mathrm{w}} .$$

Considering that the uncertain unit quaternions disperse on the hypersphere, we use the inverse arc length as the metric $\mathcal{D}(\mathbf{x}_1, \mathbf{x}_2) = 1/\operatorname{acos}\left(|\mathbf{x}_1^\top \mathbf{x}_2|\right)$. Here, the absolute value of the inner product is used to handle the antipodal symmetry of unit quaternion density. The number of neighboring grid points Λ can be flexibly adjusted when invoking the nearest neighbor search. In practice, it is not recommended to use small values of Λ for low grid resolutions. For example, searching for only one nearest neighbor can be problematic

Algorithm 2: MCG-based Discrete Quaternion Filter

Input: weighted grid points $\{(\boldsymbol{\beta}_i^k, \omega_i^k)\}_{i=1}^n$, noise samples $\{(\boldsymbol{\sigma}_r, \omega_r^{\mathrm{w}})\}_{r=1}^{n_{\mathrm{w}}}$, measurement $\mathbf{z}_{k+1}$
Output: weighted grid points $\{(\boldsymbol{\beta}_i^{k+1}, \omega_i^{k+1})\}_{i=1}^n$

/* propagate grid with noise particles */
1 $\{(\boldsymbol{\gamma}_j, \omega_j^{\mathrm{p}})\}_{j=1}^{n_{\mathrm{p}}} \leftarrow \mathtt{prop}\left(\{(\boldsymbol{\beta}_i^k, \omega_i^k)\}, \{(\boldsymbol{\sigma}_r, \omega_r^{\mathrm{w}})\}\right)$;
/* transport grid to the new mode */
2 $\boldsymbol{\nu}^{\mathrm{e}} \leftarrow \mathtt{computeMode}\left(\{(\boldsymbol{\beta}_i^k, \omega_i^k)\}\right)$;
3 $\boldsymbol{\nu}^{\mathrm{p}} \leftarrow \mathtt{computeMode}\left(\{(\boldsymbol{\gamma}_j, \omega_j^{\mathrm{p}})\}\right)$;
4 $\{\boldsymbol{\beta}_i^{k+1}\}_{i=1}^n \leftarrow \mathtt{transportGrid}\left(\{\boldsymbol{\beta}_i^k\}, \boldsymbol{\nu}^{\mathrm{e}}, \boldsymbol{\nu}^{\mathrm{p}}\right)$;
/* distribute weights to the shifted grid */
5 $\{\omega_i^{k+1}\}_{i=1}^n \leftarrow \mathtt{setElement}\,(0)$;
6 **for** $j \leftarrow 1$ **to** n_p **do**
7 $\quad \{\lambda_s\}_{s=1}^{\Lambda} \leftarrow \mathtt{searchNearest}\left(\boldsymbol{\gamma}_j, \{\boldsymbol{\beta}_i^{k+1}\}, \Lambda\right)$;
8 $\quad$ **for** $s \leftarrow 1$ **to** Λ **do**
9 $\quad\quad \omega_{\lambda_s}^{k+1} \leftarrow \omega_{\lambda_s}^{k+1} + \frac{\mathcal{D}\left(\boldsymbol{\beta}_{\lambda_s}^{k+1}, \boldsymbol{\gamma}_j\right)}{\sum_{s=1}^{\Lambda} \mathcal{D}\left(\boldsymbol{\beta}_{\lambda_s}^{k+1}, \boldsymbol{\gamma}_j\right)} \omega_j^{\mathrm{p}}$;
10 $\quad$ **end**
11 **end**
/* update grid weights with likelihood */
12 **for** $i \leftarrow 1$ **to** n **do**
13 $\quad l_i \leftarrow \mathtt{computeLikelihood}\left(\boldsymbol{\beta}_i^{k+1}, \mathbf{z}_{k+1}\right)$;
14 $\quad \omega_i^{k+1} \leftarrow \omega_i^{k+1} \times l_i$;
15 **end**
16 **return** $\{(\boldsymbol{\beta}_i^{k+1}, \omega_i^{k+1})\}_{i=1}^n$;

when the grid is propagated by system noise of relatively small disturbances, leading to no or only a tiny change to the discrete density. The mode can be obtained by calculating the weighted mean direction or by taking the grid point of the highest weight.

Given the measurement $\mathbf{z}_k$, the posterior density can be derived according to Bayes' rule as

$$\begin{aligned} f(\mathbf{x}_k \,|\, \mathbf{z}_k) &\propto f(\mathbf{z}_k \,|\, \mathbf{x}_k) \cdot f_{\mathrm{p}}(\mathbf{x}_k) \\ &= \textstyle\sum_{i=1}^n \omega_i^k \, f(\mathbf{z}_k \,|\, \boldsymbol{\beta}_i^k) \, \delta\left(\mathbf{x}_k - \boldsymbol{\beta}_i^k\right) , \end{aligned} \tag{7}$$

with $f(\mathbf{z}_k \,|\, \boldsymbol{\beta}_i)$ being the likelihood evaluated at each grid point of the prior density. The grid weights are then updated accordingly (shown in Alg. 2, lines 12–15). Usually, the mode of the discrete density changes due to the update step. For cases in which a high tracking accuracy is desired, it is thus recommended to transport the grid and reallocate the grid weights thereafter.

V. Evaluation

We evaluate the proposed filtering approach with the following set-up for nonlinear rotation estimation. The system dynamics is given as an incremental rotation of angle θ_k^{w} around axis $\boldsymbol{\zeta}_k^{\mathrm{w}}$. Both of the components entail uncertainty and are modeled by distributions from directional statistics. The rotation angle is assumed to be von Mises-distributed, i.e., $\theta_k^{\mathrm{w}} \sim \mathcal{VM}\left(\mu_\theta^{\mathrm{w}}, \kappa_\theta^{\mathrm{w}}\right)$. Similarly, the rotation axis is assumed to follow a von Mises-Fisher distribution with $\boldsymbol{\zeta}_k^{\mathrm{w}} \sim \mathcal{VMF}\left(\boldsymbol{\mu}_\zeta^{\mathrm{w}}, \kappa_\zeta^{\mathrm{w}}\right)$. The system equation can then be derived according to the quaternion parameterization as

$$\mathbf{x}_{k+1} = \mathbf{x}_k \otimes \left[\, \cos\left(\theta_k^{\mathrm{w}}/2\right), \boldsymbol{\zeta}_k^{\mathrm{w}\top} \sin\left(\theta_k^{\mathrm{w}}/2\right) \right]^\top .$$

Given the starting position $\mathbf{s}_0$, the current position via rotation of the quaternion state is measured by

$$\mathbf{z}_k = \left(\mathbf{x}_k \otimes \left[\, 0, \mathbf{s}_0^\top \,\right]^\top \otimes \mathbf{x}_k^*\right)_{2:4} + \mathbf{v}_k \,,$$

with an additive measurement noise following a zero-mean Gaussian distribution, namely, $\mathbf{v}_k \sim \mathcal{N}(\boldsymbol{\mu}^{\mathrm{v}}, \boldsymbol{\Sigma}^{\mathrm{v}})$. The corresponding likelihood function for (7) is given by $f(\mathbf{z}_k \,|\, \mathbf{x}_k) = f_{\mathbf{v}_k}\left(\mathbf{z}_k - \left(\mathbf{x}_k \otimes \left[\, 0, \mathbf{s}_0^\top \,\right]^\top \otimes \mathbf{x}_k^*\right)_{2:4}\right)$. The set-up above can be interpreted as rotating an object from its starting position $\mathbf{s}_0$ with uncertain axis-angle input $(\theta_k^{\mathrm{w}}, \boldsymbol{\zeta}_k^{\mathrm{w}})$ while observing its current position. During the prediction step of the quaternion filter, we use a constant system input according to the mean of the uncertain axis-angle rotation, i.e., $\mathbf{u}_k = \left[\, \cos\left(\mu_\theta^{\mathrm{w}}/2\right), \boldsymbol{\mu}_\zeta^{\mathrm{w}\top} \sin\left(\mu_\theta^{\mathrm{w}}/2\right) \right]^\top$.

The proposed grid-based quaternion filter (GQF) is then compared with existing on-manifold quaternion filtering schemes, which all assume the underlying uncertainty to be Bingham-distributed. Different sampling schemes can be applied to the Bingham quaternion filter (BQF) for handling the nonlinear set-up above. Here, we exploit the BQFs based on deterministic (Det-BQF) [22] as well as random samples (Rnd-BQF) [23]. Additionally, we utilize deterministic sampling in a progressive filtering scheme [31], [32] (Prg-Det-BQF) for further benchmarking the performance of nonlinear quaternion filtering. Here, 1000 deterministic samples are used in the Det-BQF for both prediction and update steps. The Prg-Det-BQF also relies on 1000 deterministic samples in the prediction step, whereas 50 deterministic samples are used for progressive update steps. The Rnd-BQF uses 2000 random samples. Finally, the proposed GQF is based on a grid of $L = 30$ layers with $M = 30$ layer-wise points, leading to a grid with only 901 points. The uncertainty of the system dynamics is fixed as $\kappa_\theta^{\mathrm{w}} = \kappa_\zeta^{\mathrm{w}} = 50$, and the aforementioned approaches are compared under different levels of measurement noise of $\boldsymbol{\Sigma}^{\mathrm{v}} = c \cdot \mathbf{I}_{3\times 3}$, with $c \in \{\,0.1, 0.05, 0.001\}$.

The simulation is performed based on 100 Monte Carlo runs of 50 steps. To illustrate the estimates more intuitively, the quaternion state is mapped to the measurement space via the observation equation $\hat{\mathbf{z}}_k = \left(\hat{\mathbf{x}}_k \otimes \left[\, 0, \mathbf{s}_0^\top \,\right]^\top \otimes \hat{\mathbf{x}}_k^*\right)_{2:4}$, which is then compared with the one given by the ground truth. The errors are plotted using the `boxplot` function in MATLAB. Note the measurements have the same DoF as the quaternion states. Thus, using such a mapping for demonstrating tracking accuracy does not conceal error. As shown in Fig. 3, the proposed GQF shows superior tracking accuracy and is more computationally efficient than the other approaches. The estimation quality is improved mainly because the underlying state uncertainty is no longer Bingham-distributed and cannot be modeled in a parametric form. Particularly, low measurement uncertainties (e.g., by using an accurate sensor) lead to a peaky likelihood function. In this case, the samples drawn from the Bingham-distributed prior degenerate more easily when they are updated, resulting in total failures of the other approaches as shown in Fig. 3 (c).

For the medium noise level, we evaluate the proposed GQF with different grid resolutions of $L = M \in \{10, 20, 40, 60\}$.

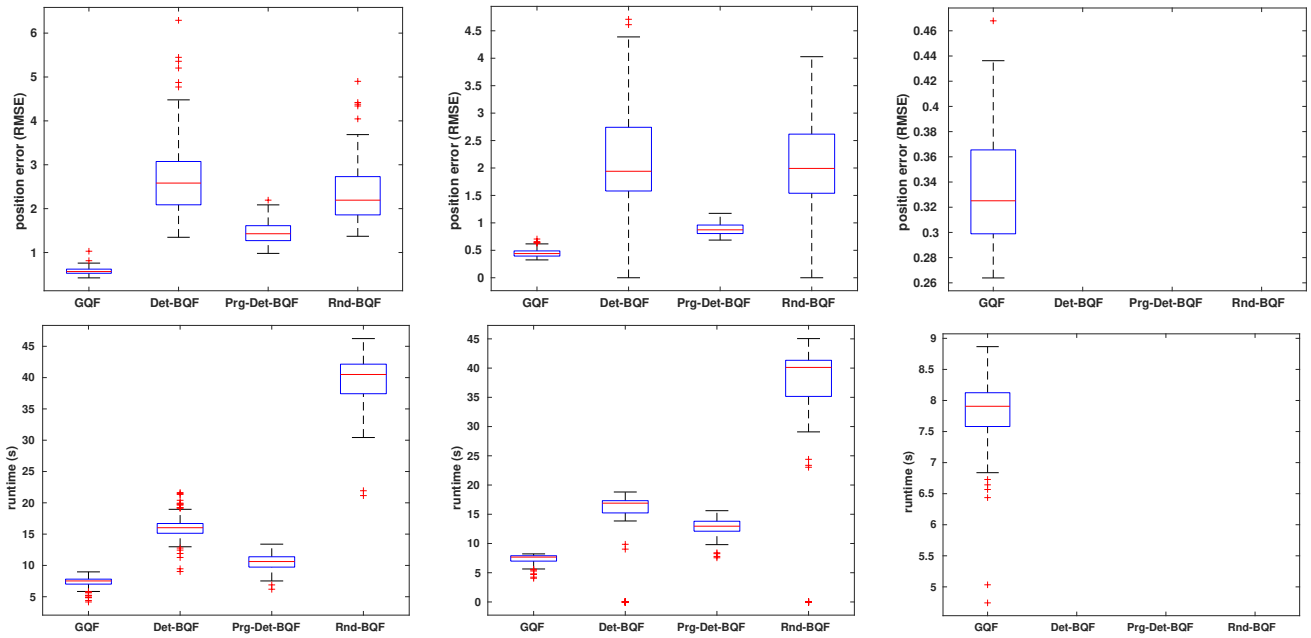

(a) large noise (b) medium noise (c) low noise

Fig. 3: Comparison of the proposed grid-based quaternion filter with existing on-manifold quaternion filtering approaches under different measurement noise levels. The proposed GQF shows superior tracking performance w.r.t. accuracy and computational efficiency as well as robustness.

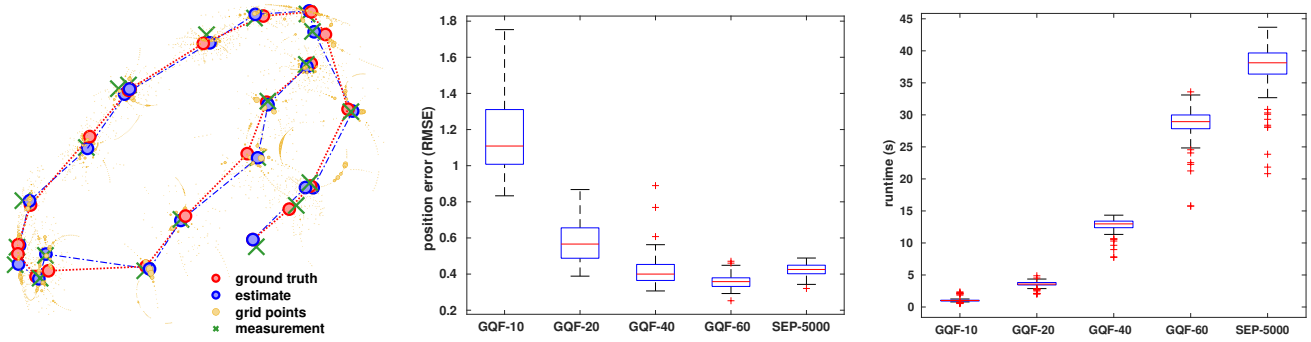

(a) (b) (c)

Fig. 4: (a): Illustration of a segment of a representative run using the proposed MCG-based quaternion filter. Dashed lines only indicate the change of locations from one time stamp to the next. (b)–(c): Tracking performance comparison of the proposed grid-based quaternion filters with different grid resolutions.

A segment of an exemplary run given by the proposed MCG-based quaternion filter is shown in Fig. 4 (a). At each step, weighted grid points of the posterior are also depicted in the measurement space. As shown in Fig. 4 (b)-(c), higher grid resolutions give better tracking accuracy while demanding more runtime. A similar filtering scheme without grid transport using a grid from the original SEP algorithm is also tested. However, the SEP-based approach with 5000 grid points still performs slightly worse and is much slower than the MCG-based filter with $40^2+1=1601$ grid points. This is not surprising as the MCG has a more efficient modeling of uncertainty, as shown in Sec. III .

VI. Conclusion

In this work, we introduce a novel discrete quaternion filter for SO(3) estimation. A mode-centric grid is proposed based on spherical geometry to discretize the unit quaternion manifold for efficient representation of the underlying uncertainty via Dirac mixtures. The grid-based quaternion filter does not require the noise density to be given in parametric form and shows superior tracking accuracy and robustness compared with existing Bingham-based filters.

Further potential of the discrete quaternion filter can still be exploited. For instance, the state space can be extended to other manifolds, e.g., products of hyperspheres (for articulated robot kinematics) or the manifold representing the six-DoF rigid body transformations. Also, the grid can be generated and stored in a more structured way (e.g., using space partitioning algorithms), such that grid points can be retrieved faster and the runtime can be further reduced.

APPENDIX

A. Derivation of the Grid-Based Prior

Based on the chain rule for the probability density function, the prior represented by grid points is formulated as

$$\begin{aligned} &f_{\mathrm{p}}(\mathbf{x}_{k+1}) = \textstyle\int_{\mathbb{S}^3} \int_{\mathbb{W}} f(\mathbf{x}_{k+1}, \mathbf{x}_k, \mathbf{w}_k)\, d\mathbf{w}_k\, d\mathbf{x}_k \\ &= \textstyle\int_{\mathbb{S}^3} f_{\mathrm{e}}(\mathbf{x}_k) \int_{\mathbb{W}} f(\mathbf{x}_{k+1}, \mathbf{w}_k \,|\, \mathbf{x}_k)\, d\mathbf{w}_k\, d\mathbf{x}_k \\ &= \textstyle\int_{\mathbb{S}^3} f_{\mathrm{e}}(\mathbf{x}_k) \int_{\mathbb{W}} \delta\left(\mathbf{x}_{k+1} - a(\mathbf{x}_k, \mathbf{w}_k)\right) f_{\mathrm{w}}(\mathbf{w}_k)\, d\mathbf{w}_k\, d\mathbf{x}_k\,. \end{aligned}$$

Here, the posterior of the previous step and the noise density are both given in discrete form, i.e., $f_{\mathrm{e}}(\mathbf{x}_k) = \sum_{i=1}^{n} \omega_i^k\, \delta\left(\mathbf{x}_k - \boldsymbol{\beta}_i^k\right)$ and $f_{\mathrm{w}}(\mathbf{w}_k) = \sum_{r=1}^{n_{\mathrm{w}}} \omega_r^{\mathrm{w}}\, \delta\left(\mathbf{w}_k - \boldsymbol{\sigma}_r\right)$. The prior can thus be further derived as follows

$$\begin{aligned} f_{\mathrm{p}}(\mathbf{x}_{k+1}) &= \textstyle\int_{\mathbb{S}^3} \sum_{i=1}^{n} \omega_i^k\, \delta\left(\mathbf{x}_k - \boldsymbol{\beta}_i^k\right) \\ &\qquad \cdot \textstyle\sum_{r=1}^{n_{\mathrm{w}}} \omega_r^{\mathrm{w}}\, \delta\left(\mathbf{x}_{k+1} - a(\mathbf{x}_k, \boldsymbol{\sigma}_r)\right)\, d\mathbf{x}_k \\ &\approx \textstyle\sum_{i=1}^{n} \sum_{r=1}^{n_{\mathrm{w}}} \omega_i^k\, \omega_r^{\mathrm{w}}\, \delta\left(\mathbf{x}_{k+1} - a\left(\boldsymbol{\beta}_i^k, \boldsymbol{\sigma}_r\right)\right)\,, \end{aligned}$$

which is approximated by the propagated grid points.

REFERENCES

[1] K. Sun, K. Mohta, B. Pfrommer, M. Watterson, S. Liu, Y. Mulgaonkar, C. J. Taylor, and V. Kumar, "Robust Stereo Visual Inertial Odometry for Fast Autonomous Flight," *IEEE Robotics and Automation Letters (RA-L)*, vol. 3, no. 2, pp. 965–972, 2018.

[2] H. A. Hashim, L. J. Brown, and K. A. McIsaac, "Guaranteed Performance of Nonlinear Attitude Filters on the Special Orthogonal Group SO(3)," *IEEE Access*, vol. 7, pp. 3731–3745, 2019.

[3] H. A. Hashim, L. J. Brown, and K. McIsaac, "Guaranteed Performance of Nonlinear Pose Filter on SE(3)," in *Proceedings of the 2019 American Control Conference (ACC 2019)*, Philadelphia, PA, USA, July 2019, pp. 1–6.

[4] T. Johansen, T. S. Andersen, and R. Kristiansen, "PD+ Based Trajectory Tracking of the Underactuated Quadrotor Platform using Dual Quaternions," in *Proceedings of the 2019 American Control Conference (ACC 2019)*, Philadelphia, PA, USA, July 2019, pp. 1342–1348.

[5] X. Zhu, X. Liu, Z. Lei, and S. Z. Li, "Face Alignment in Full Pose Range: A 3D Total Solution," *IEEE Transactions on Pattern Analysis and Machine Intelligence*, vol. 41, no. 1, pp. 78–92, 2019.

[6] C. Jahanchahi and D. P. Mandic, "A Class of Quaternion Kalman Filters," *IEEE Transactions on Neural Networks and Learning Systems*, vol. 25, no. 3, pp. 533–544, March 2014.

[7] S. J. Julier and J. K. Uhlmann, "Unscented Filtering and Nonlinear Estimation," *Proceedings of the IEEE*, vol. 92, no. 3, pp. 401–422, 2004.

[8] M. Bloesch, M. Burri, S. Omari, M. Hutter, and R. Siegwart, "Iterated Extended Kalman Filter Based Visual-Inertial Odometry Using Direct Photometric Feedback," *The International Journal of Robotics Research*, vol. 36, no. 10, pp. 1053–1072, 2017.

[9] S. Hauberg, F. Lauze, and K. S. Pedersen, "Unscented Kalman Filtering on Riemannian Manifolds," *Journal of Mathematical Imaging and Vision*, vol. 46, no. 1, pp. 103–120, 2013.

[10] C. Forster, L. Carlone, F. Dellaert, and D. Scaramuzza, "On-Manifold Preintegration for Real-Time Visual–Inertial Odometry," *IEEE Transactions on Robotics*, vol. 33, no. 1, pp. 1–21, 2016.

[11] M. H. Moghari and P. Abolmaesumi, "Point-Based Rigid-body Registration Using an Unscented Kalman Filter," *IEEE Transactions on Medical Imaging*, vol. 26, no. 12, pp. 1708–1728, 2007.

[12] R. Arun Srivatsan, M. Xu, N. Zevallos, and H. Choset, "Probabilistic Pose Estimation Using a Bingham Distribution-Based Linear Filter," *The International Journal of Robotics Research*, vol. 37, no. 13-14, pp. 1610–1631, 2018.

[13] K. V. Mardia and P. E. Jupp, *Directional Statistics*. John Wiley & Sons, 2009, vol. 494.

[14] R. A. Srivatsan, G. T. Rosen, D. F. N. Mohamed, and H. Choset, "Estimating SE(3) Elements Using a Dual Quaternion Based Linear Kalman Filter," in *Proceedings of Robotics: Science and Systems (RSS 2016)*, Boston,USA, 2016.

[15] J. Glover, G. Bradksi, and R. Rusu, "Monte Carlo Pose Estimation with Quaternion Kernels and the Bingham Distribution," in *Proceedings of Robotics: Science and Systems*, Los Angeles, CA, USA, June 2012.

[16] K. Li, G. Kurz, L. Bernreiter, and U. D. Hanebeck, "Simultaneous Localization and Mapping Using a Novel Dual Quaternion Particle Filter," in *Proceedings of the 21st International Conference on Information Fusion (Fusion 2018)*, Cambridge, United Kingdom, July 2018.

[17] K. Li, F. Pfaff, and U. D. Hanebeck, "Geometry-Driven Stochastic Modeling of SE(3) States Based on Dual Quaternion Representation," in *Proceedings of the 2019 IEEE International Conference on Multisensor Fusion and Integration for Intelligent Systems (MFI 2019)*, Taipei, Republic of China, May 2019.

[18] K. Li, G. Kurz, L. Bernreiter, and U. D. Hanebeck, "Nonlinear Progressive Filtering for SE(2) Estimation," in *Proceedings of the 21st International Conference on Information Fusion (Fusion 2018)*, Cambridge, United Kingdom, July 2018.

[19] J. Glover and L. P. Kaelbling, "Tracking the Spin on a Ping Pong Ball with the Quaternion Bingham Filter," in *2014 IEEE International Conference on Robotics and Automation (ICRA 2014)*, May 2014, pp. 4133–4140.

[20] I. Gilitschenski, G. Kurz, S. J. Julier, and U. D. Hanebeck, "Unscented Orientation Estimation Based on the Bingham Distribution," *IEEE Transactions on Automatic Control*, vol. 61, no. 1, pp. 172–177, Jan. 2016.

[21] K. Li, D. Frisch, B. Noack, and U. D. Hanebeck, "Geometry-Driven Deterministic Sampling for Nonlinear Bingham Filtering," in *Proceedings of the 2019 European Control Conference (ECC 2019)*, Naples, Italy, June 2019.

[22] K. Li, F. Pfaff, and U. D. Hanebeck, "Hyperspherical Deterministic Sampling Based on Riemannian Geometry for Improved Nonlinear Bingham Filtering," in *Proceedings of the 22nd International Conference on Information Fusion (Fusion 2019)*, Ottawa, Canada, July 2019.

[23] J. M. Glover, "The Quaternion Bingham Distribution, 3D Object Detection, and Dynamic Manipulation," Ph.D. dissertation, Massachusetts Institute of Technology, 2014.

[24] I. Gilitschenski, G. Kurz, S. J. Julier, and U. D. Hanebeck, "Efficient Bingham Filtering based on Saddlepoint Approximations," in *Proceedings of the 2014 IEEE International Conference on Multisensor Fusion and Information Integration (MFI 2014)*, Beijing, China, Sept. 2014.

[25] S. Bultmann, K. Li, and U. D. Hanebeck, "Stereo Visual SLAM Based on Unscented Dual Quaternion Filtering," in *Proceedings of the 22nd International Conference on Information Fusion (Fusion 2019)*, Ottawa, Canada, July 2019.

[26] W. M. Wonham, "Some Applications of Stochastic Differential Equations to Optimal Nonlinear Filtering," *Journal of the Society for Industrial and Applied Mathematics, Series A: Control*, vol. 2, no. 3, pp. 347–369, 1964.

[27] G. Kurz, F. Pfaff, and U. D. Hanebeck, "Application of Discrete Recursive Bayesian Estimation on Intervals and the Unit Circle to Filtering on SE(2)," *IEEE Transactions on Industrial Informatics*, vol. 14, no. 3, pp. 1197–1206, Mar. 2018.

[28] F. Pfaff, K. Li, and U. D. Hanebeck, "Fourier Filters, Grid Filters, and the Fourier-Interpreted Grid Filter," in *Proceedings of the 22nd International Conference on Information Fusion (Fusion 2019)*, Ottawa, Canada, July 2019.

[29] P. Leopardi, "A Partition of the Unit Sphere Into Regions of Equal Area and Small Diameter," *Electronic Transactions on Numerical Analysis*, vol. 25, no. 12, pp. 309–327, 2006.

[30] G. Kurz and U. D. Hanebeck, "Linear Regression Kalman Filtering Based on Hyperspherical Deterministic Sampling," in *Proceedings of the 56th IEEE Conference on Decision and Control (CDC 2017)*, Melbourne, Australia, Dec. 2017.

[31] U. D. Hanebeck, K. Briechle, and A. Rauh, "Progressive Bayes: A New Framework for Nonlinear State Estimation," in *Proceedings of SPIE, AeroSense Symposium*, vol. 5099, Orlando, Florida, USA, May 2003, pp. 256 – 267.

[32] K. Li, D. Frisch, S. Radtke, B. Noack, and U. D. Hanebeck, "Wavefront Orientation Estimation Based on Progressive Bingham Filtering," in *Proceedings of the IEEE ISIF Workshop on Sensor Data Fusion: Trends, Solutions, Applications (SDF 2018)*, Oct. 2018.